

# Probing Protein Ligand Interactions by Automated Hydrogen/Deuterium Exchange Mass Spectrometry

Michael J. Chalmers,<sup>†</sup> Scott A. Busby,<sup>†</sup> Bruce D. Pascal,<sup>†</sup> Yuanjun He,<sup>†</sup> Christopher L. Hendrickson,<sup>‡,§</sup> Alan G. Marshall,<sup>‡,§</sup> and Patrick R. Griffin<sup>\*,†</sup>

The Scripps Research Institute, 5353 Parkside Drive (RF-1), Jupiter, Florida 33458, National High Magnetic Field Laboratory, Florida State University, 1800 East Paul Dirac Drive, Tallahassee, Florida 32310-4005, and Department of Chemistry and Biochemistry, Florida State University, Tallahassee, Florida 32306

Amide hydrogen/deuterium exchange is a powerful biophysical technique for probing changes in protein dynamics induced by ligand interaction. The inherent low throughput of the technology has limited its impact on drug screening and lead optimization. Automation increases the throughput of H/D exchange to make it compatible with drug discovery efforts. Here we describe the first fully automated H/D exchange system that provides highly reproducible H/D exchange kinetics from 130 ms to 24 h. Throughput is maximized by parallel sample processing, and the system can run H/D exchange assays in triplicate without user intervention. We demonstrate the utility of this system to differentiate structural perturbations in the ligand-binding domain (LBD) of the nuclear receptor PPAR $\gamma$  induced upon binding a full agonist and a partial agonist. PPAR $\gamma$  is the target of glitazones, drugs used for treatment of insulin resistance associated with type II diabetes. Recently it has been shown that partial agonists of PPAR $\gamma$  have insulin sensitization properties while lacking several adverse effects associated with full agonist drugs. To further examine the mechanism of partial agonist activation of PPAR $\gamma$ , we extended our studies to the analysis of ligand interactions with the heterodimeric complex of PPAR $\gamma$ /RXR $\alpha$  LBDs. To facilitate analysis of H/D exchange of large protein complexes, we performed the experiment with a 14.5-T Fourier transform ion cyclotron resonance mass spectrometer capable of measuring mass with accuracy in the ppb range.

**Hydrogen/Deuterium Exchange (H/D Exchange).** Proteins are the target of most therapeutic agents. Understanding the nature of the interactions these agents make with their target proteins has proven powerful in aiding drug discovery and drug development. Although many biophysical methods measure characteristic protein properties, most of these techniques, such as circular dichroism, differential scanning calorimetry, and ultracentrifugation, provide mainly global information. X-ray crystallography and nuclear magnetic resonance (NMR) provide

localized, high-resolution structural information on proteins and protein–ligand interactions. The utility of both crystallography and NMR is well recognized, and substantial efforts to further develop and utilize these technologies for screening are underway. However, both techniques have limitations. In crystallography, crystallization remains the major obstacle and certain proteins, including many membrane proteins and intrinsically disordered proteins, are inherently noncrystallizable. Even with state-of-the-art high-field magnets, selective labeling methods, and new pulse sequences, many proteins are too large for analysis by NMR. In addition, for both techniques, proteins can be studied only under a limited set of conditions, such as in the solid state for crystallography and at high concentrations for NMR.

Amide H/D exchange has proven to be useful for the study of protein structure and dynamics as well as protein–ligand interactions.<sup>1–21</sup> The degree to which an amide hydrogen is

- (1) Englander, S. W.; Kallenbach, N. R. *Q. Rev. Biophys.* **1983**, *16* (4), 521–655.
- (2) Bai, Y. W.; Milne, J. S.; Mayne, L.; Englander, S. W. *Proteins: Struct., Funct., Genet.* **1993**, *17* (1), 75–86.
- (3) Zhang, Z.; Smith, D. L. *Protein Sci.* **1993**, *2* (4), 522–531.
- (4) Chamberlain, A. K.; Marqusee, S. *Structure* **1997**, *5* (7), 859–863.
- (5) Englander, S. W.; Mayne, L.; Bai, Y.; Sosnick, T. R. *Protein Sci.* **1997**, *6* (5), 1101–1109.
- (6) Engen, J. R.; Smith, D. L. *Anal. Chem.* **2001**, *73* (9), 256A–265A.
- (7) Sivaraman, T.; Arrington, C. B.; Robertson, A. D. *Nat. Struct. Biol.* **2001**, *8* (4), 331–333.
- (8) Hamuro, Y.; Wong, L.; Shaffer, J.; Kim, J. S.; Stranz, D. D.; Jennings, P. A.; Woods, V. L.; Adams, J. A. *J. Mol. Biol.* **2002**, *323* (5), 871–881.
- (9) Hamuro, Y.; Zawadzki, K. M.; Kim, J. S.; Stranz, D. D.; Taylor, S. S.; Woods, V. L. *J. Mol. Biol.* **2003**, *327* (5), 1065–1076.
- (10) Hamuro, Y.; Coales, S. J.; Southern, M. R.; Griffin, P. R. *Protein Sci.* **2004**, *13*, 141–141.
- (11) Yan, X. G.; Broderick, D.; Leid, M. E.; Schimerlik, M. I.; Deinzer, M. L. *Biochemistry* **2004**, *43* (4), 909–917.
- (12) Yan, X. G.; Watson, J.; Ho, P. S.; Deinzer, M. L. *Mol. Cell. Proteomics* **2004**, *3* (1), 10–23.
- (13) Garcia, R. A.; Pantazatos, D.; Villarreal, F. J. *Assay Drug Dev. Technol.* **2004**, *2* (1), 81–91.
- (14) Lisal, J.; Lam, T. T.; Kainov, D. E.; Emmett, M. R.; Marshall, A. G.; Tuma, R. *Nat. Struct. Mol. Biol.* **2005**, *12* (5), 460–466.
- (15) Busenlehner, L. S.; Armstrong, R. N. *Arch. Biochem. Biophys.* **2005**, *433* (1), 34–46.
- (16) Nazabal, A.; Maddelein, M. L.; Bonneau, M.; Saupe, S. J.; Schmitter, J. M. *J. Biol. Chem.* **2005**, *280* (14), 13220–13228.
- (17) Winters, M. S.; Spellman, D. S.; Lambiris, J. D. *J. Immunol.* **2005**, *174* (6), 3469–3474.
- (18) Mandell, J. G.; Baerga-Ortiz, A.; Falick, A. M.; Komives, E. A. *Methods Mol. Biol.* **2005**, *305*, 65–80.
- (19) Mandell, J. G.; Falick, A. M.; Komives, E. A. *Proc. Natl. Acad. Sci. U.S.A.* **1998**, *95* (25), 14705–14710.

\* To whom correspondence should be addressed. E-mail: pgriffin@scripps.edu.

<sup>†</sup> The Scripps Research Institute.

<sup>‡</sup> National High Magnetic Field Laboratory, Florida State University.

<sup>§</sup> Department of Chemistry and Biochemistry, Florida State University.

exposed to solvent reveals much about its environment. Conformational change induced by ligand binding causes variations in amide exposure, and these variations can be determined by measuring the rate of amide hydrogen exchange with solvent deuterium. Mass spectrometry (MS)-based H/D exchange approaches can measure the rate of amide hydrogen exchange with solvent in defined regions of a protein, and this technology offers flexibility in measuring exchange kinetics under nearly unlimited solution conditions and protein concentrations. Typically, H/D exchange analysis involves exposing the protein to a deuterated environment for a predefined time period (referred to as on-exchange) followed by immediate addition of a quench buffer (low pH, low temperature) containing denaturants to significantly slow further on-exchange of deuterium and to minimize back-exchange with nondeuterated solvent. Deuterated and denatured protein is digested with acid-stable proteases, and the uptake of deuterium in specific regions of the protein is determined by liquid chromatography electrospray ionization mass spectrometry (LC-ESI-MS) by measuring the increase in number-average  $m/z$  values of peptide ion isotopic distributions for each peptide that can be monitored. To probe protein–ligand interactions, these experiments are performed on both the free protein and protein–ligand complex. The difference in area under plots of deuterium uptake versus exchange-on period for the two experiments (free versus ligand bound) reveals regions in the protein that possess differential exchange kinetics as a result of ligand interaction. The resulting differential exchange map serves as a fingerprint for that specific protein–ligand interaction. These fingerprints can be used to identify and cluster ligands that interact with the target protein in a specific mode. Thus, H/D exchange MS fills an existing gap in protein analysis methods and has evolved into an effective method for probing protein–ligand interactions. Unfortunately, H/D exchange MS has not yet realized its full potential in screening protein–ligand interactions due to several technical challenges. To that end, we have developed an automated H/D exchange MS platform, which is described below, and we have applied that platform to the analysis of ligand interactions with the ligand-dependent nuclear receptors, PPAR $\gamma$  and RXR $\alpha$ .

**Probing Ligand Interactions with the Peroxisome Proliferator-Activated Receptor  $\gamma$  Ligand-Binding Domain (PPAR $\gamma$  LBD).** In recent years, there has been intensive research into understanding the mechanism of ligand-mediated activation of nuclear receptors.<sup>22</sup> The increased interest in this area has been driven in part by the success of targeting nuclear receptors for treatment of a wide range of diseases such as type II diabetes, cancer, cardiovascular disease, and hormone replacement therapy. Marketed drugs that target the nuclear receptors, PPAR $\alpha$ , PPAR $\gamma$ , GR, and ER, have shown clinical efficacy, but often are accompanied by an array of mechanism-based side effects. For example, full agonists of PPAR $\gamma$ , drugs known as the glitazones, are insulin-sensitizing agents used effectively in treatment of type II diabetes. However, clinical use of glitazones is associated with side effects such as weight gain, plasma volume expansion, and edema. These unwanted effects limit the utility of PPAR $\gamma$  agonists in chronic treatment of insulin resistance.

Recent information on the mechanism of activation of nuclear receptors has led to the proposal that selective nuclear receptor modulators, S(NR)Ms, can be developed.<sup>23,24</sup> Examples have been the development of selective estrogen receptor modulators or SERMs<sup>25</sup> and selective PPAR $\gamma$  modulators or SPPAR $\gamma$ Ms.<sup>26</sup> Ligand-dependent activation of nuclear receptors involves conformational change in the receptor induced by ligand binding. The ligand-induced conformational change can drive dissociation of repressor molecules and the recruitment of activator molecules. This dynamic process is difficult to measure in the context of the receptor by most structural technologies. Thus, we have developed automated H/D exchange MS to probe conformational changes induced by ligand binding to nuclear receptors.

Previously, Yan and colleagues utilized H/D exchange to probe the solution conformation of the retinoid X receptor  $\alpha$  LBD (RXR $\alpha$  LBD) in the presence and absence of 9-*cis*-retinoic acid (9-*cis*-RA).<sup>11</sup> In those studies, perturbation in H/D exchange of RXR $\alpha$  LBD upon 9-*cis*-RA binding correlated well with changes in hydrogen bonding, amino acid residue depth, and solvent exposure predicted from the co-crystal structure.<sup>27</sup> However, perturbation in exchange kinetics was also observed in regions not predicted from the X-ray structure. That work highlights the complementary relation between H/D exchange and X-ray crystallography, and it demonstrates the utility of H/D exchange for probing drug interactions with nuclear receptors.

**Fourier Transform Ion Cyclotron Resonance Mass Spectrometry.** The success of the H/D exchange experiment depends on the ability to measure the increase in number-average  $m/z$  values of peptide ion isotopic distributions following incubation of the intact protein with deuterium oxide for various periods of time. Low-resolution mass analyzers such as linear quadrupole ion traps rely on efficient chromatographic separation to ensure that peptide ions do not simultaneously overlap in  $m/z$  and chromatographic retention time. Unfortunately, the rapid rate of D/H back exchange, even under slow exchange conditions, limits the chromatographic step to less than 30 min. Even the analysis of relatively small proteins (20–30 kDa) leads to several overlapping isotopic distributions. With the limited resolving power of the linear quadrupole ion trap, those peptides cannot be included in the on-exchange data set.

Fourier transform ion cyclotron resonance mass spectrometry<sup>28</sup> provides the highest available resolving power and mass accuracy of any mass analyzer.<sup>29</sup> The resolution is sufficient to determine number-average  $m/z$  values from overlapping isotopic distributions, thereby increasing information content from H/D exchange

(20) Carter, J. M.; Gurevich, V. V.; Prossnitz, E. R.; Engen, J. R. *J. Mol. Biol.* **2005**, *351* (4), 865–878.

(21) Engen, J. R. *Analyst* **2003**, *128* (6), 623–628.

(22) Gronemeyer, H.; Gustafsson, J. A.; Laudet, V. *Nat. Rev. Drug Discovery* **2004**, *3* (11), 950–964.

(23) Jordan, V. C. *J. Med. Chem.* **2003**, *46* (7), 1081–1111.

(24) Jordan, V. C. *J. Med. Chem.* **2003**, *46* (6), 883–908.

(25) Goldfrank, D.; Haytuglu, T.; Frishman, W. H.; Mohammad, Z. *J. Clin. Pharmacol.* **1999**, *39* (8), 767–774.

(26) Berger, J. P.; Petro, A. E.; Macnaul, K. L.; Kelly, L. J.; Zhang, B. B.; Richards, K.; Elbrecht, A.; Johnson, B. A.; Zhou, G.; Doebber, T. W.; Biswas, C.; Parikh, M.; Sharma, N.; Tanen, M. R.; Thompson, G. M.; Ventre, J.; Adams, A. D.; Mosley, R.; Surwit, R. S.; Moller, D. E. *Mol. Endocrinol.* **2003**, *17* (4), 662–676.

(27) Egea, J.; Espinet, C.; Soler, R. M.; Peiro, S.; Rocamora, N.; Comella, J. X. *Mol. Cell. Biol.* **2000**, *20* (6), 1931–1946.

(28) Marshall, A. G.; Hendrickson, C. L.; Jackson, G. S. *Mass Spectrom. Rev.* **1998**, *17*, 1–35.

(29) Marshall, A. G.; Hendrickson, C. L.; Shi, S. D. H. *Anal. Chem.* **2002**, *74* (9), 253A–259A.

experiments. This added information increases the overall amino acid sequence coverage of the target protein and improves the spatial resolution of the experiment. Additional benefits arise from the ability to minimize the time scale of the chromatographic step,<sup>30</sup> thereby providing simultaneous increases in deuterium retention and sample throughput. For the reasons outlined above, FT-ICR is an attractive mass analyzer for H/D exchange experiments.

In this paper, we describe a fully automated system for solution-phase H/D exchange experiments capable of incubating protein with deuterium oxide for periods between 130 ms and 24 h. We demonstrate the utility of the system with a standard protein, horse heart cytochrome *c*. Furthermore, we demonstrate that we can measure changes in H/D exchange rates upon ligand binding to PPAR $\gamma$  LBD, and that we can discriminate binding interactions of full agonists from partial agonists of PPAR $\gamma$ . To further demonstrate the broad utility of this H/D exchange platform, the system was interfaced with a 14.5-T FT-ICR mass spectrometer to investigate the effects of ligand binding on the PPAR $\gamma$  LBD/RXR $\alpha$  LBD heterodimer complex.

## EXPERIMENTAL SECTION

**Materials.** Histidine-tagged wild-type PPAR $\gamma$  LBD and RXR $\alpha$  LBD were purchased from Protein One (College Park, MD) and used without further preparation. The PPAR $\gamma$  partial agonist nTZDpa was synthesized by a previously described chemical strategy and was prepared as a 10 mM stock in DMSO.<sup>33</sup> GW1929 was purchased from Sigma (St. Louis, MO). Protein dilution buffer (H<sub>2</sub>O or D<sub>2</sub>O) was 20 mM Tris-Cl, pH 7.9, containing 100 mM KCl, and 1 mM DTT. Quench solution was 2 M urea in 0.5% aqueous trifluoroacetic acid (TFA). All other chemicals and solvents were purchased from Sigma. For protein:ligand experiments, protein stock solutions (10  $\mu$ M) were incubated with ligand solution (200  $\mu$ M) for 3 h at 25 °C.

**Automated H/D Exchange.** Solution-phase H/D exchange was performed with a system constructed around a LEAP Technologies Twin PAL HTS autosampler (LEAP Technologies, Carrboro, NC). Two Peltier-cooled sample stacks (LEAP Technologies) provide for accurate control of the environment for on-exchange experiments and provide accurate control of the temperature of the quench buffer and protein stock solutions. Each stack has three drawers that hold two 96- or 384-well microtiter plates. For this work, however, we used 200- $\mu$ L silanized capped glass vials (Microliter Analytical Supplies Inc., Suwanee, GA) located in four 96-position sample trays. For manipulation of the protein solution, PAL 2 is equipped with a 10- $\mu$ L syringe (L300.0010-2, Microliter Analytical Supplies Inc.) and can aspirate and dispense solution from any location within either sample stack. For dilutions and sample injection, PAL 1 contains a 100- $\mu$ L syringe (L300.0062-2, Microliter Analytical Supplies Inc.) and can traverse between both sample stacks and the HPLC injection port. A three-valve unit (Trio valve, LEAP Technologies) constructed with a custom thermal chamber (McCour, Groveland, MA) held at 1.25

°C controls the mobile-phase flow paths such that on-line protein digestion, peptide desalting, and reversed-phase HPLC separation are performed prior to infusion into the ESI ion source of the mass spectrometer. Sample loading, digestion, and desalting (60–180 s) was driven with an isocratic HPLC pump (IPro-500, IRIS Technologies, Lawrence, KS) at a flow rate of 200  $\mu$ L min<sup>-1</sup> (0.1% TFA) through the 50- $\mu$ L sample loop, the immobilized pepsin column (Porozyme, Applied Biosystems, Foster City, CA), across a C<sub>18</sub> trap column (Peptide Microtrap, Microm Bioresources, Auburn, CA), and out to waste. After isolation of the enzyme column from the flow path, gradient elution from the trap across a self-packed POROS 20R2 column (1 mm i.d.  $\times$  1 cm) was performed with a capillary-scale HPLC pump (Agilent 1100, Palo Alto, CA). The flow rate was held constant at 60  $\mu$ L min<sup>-1</sup> while the composition of the mobile phase was increased from 4% CH<sub>3</sub>CN containing 0.3% formic acid (FA) to 40% CH<sub>3</sub>CN containing 0.3% FA over 18 min. Following gradient elution, mobile-phase composition was increased over a 1-min period to 80% CH<sub>3</sub>CN, 0.3% FA and held at that composition for 8 min prior to reduction over 1 min to 100% H<sub>2</sub>O, 0.3% FA. The valves then directed the mobile-phase flow path such that the separating column and trap column were back-flushed for 7 min. All HPLC connections were made with 1/16 in.  $\times$  0.05 in. PEEK tubing.

**On-Exchange.** To achieve H/D on-exchange exposure between 130 ms and 24 h, we operate the LEAP system in two different modes, both of which are automated and can be performed interchangeably during the same experiment. The first mode is capable of operating between 130 ms and 30 s. The second mode can perform experiments from 30 s up to 24 h (86 399 s (24 h) is the LEAP “wait timer” maximum value). To increase throughput, the LEAP macro was constructed in such a way that all long exchange time periods (>600 s) are performed in parallel with the analysis of the short on-exchange periods (<300 s) or alongside the HPLC back flush and reconditioning steps. To run 1, 15, 30, 60, 300, 900, 1800, 3600, and 12 000 s on-exchange periods in triplicate requires  $\sim$ 24 h. An equivalent experiment done in series would require  $\sim$ 36 h.

**Rapid On-Exchange Periods: 130 ms to 15 s.** Although rapid, the LEAP HTS PAL autosampler requires a finite amount of time to open and close sample drawers and move between sample vials. Therefore, to perform on-exchange experiments shorter than 15 s (the minimum interval to move between the protein vial and the quench vial), the on-exchange experiment must be performed in a single vial, without moving the syringe. To that end, we make use of the ability of the LEAP to aspirate an air gap between solutions. To initiate the experiment, PAL 2 places 4  $\mu$ L of the protein stock solution into an empty vial held at 25 °C. PAL 1 then aspirates 30  $\mu$ L of quench solution (held at 1.5 °C), followed by an air gap of 10  $\mu$ L, and finally draws up 16  $\mu$ L of the D<sub>2</sub>O on-exchange buffer (Figure 1, inset). To initiate the on-exchange, 16  $\mu$ L of D<sub>2</sub>O solution is dispensed into the sample vial at a rate of 200  $\mu$ L s<sup>-1</sup> (80 ms). For experiments between 1 and 15 s, the syringe waits for the preset period of time prior to dispensing the air gap (50 ms) and quench solution (150 ms) into the vial at 200  $\mu$ L s<sup>-1</sup>. For the 130-ms experiment, the D<sub>2</sub>O solution, air gap, and quench solution were dispensed at a rate of 200  $\mu$ L s<sup>-1</sup> with no intervening delay. Dispensing the D<sub>2</sub>O buffer requires 80 ms. and the following 10- $\mu$ L air gap creates

(30) Zhang, Z. Q.; Li, W. Q.; Logan, T. M.; Li, M.; Marshall, A. G. *Protein Sci.* **1997**, *6* (10), 2203–2217.

(31) Yang, J.; Garrod, S. M.; Deal, M. S.; Anand, G. S.; Woods, V. L.; Taylor, S. *J. Mol. Biol.* **2005**, *346* (1), 191–201.

(32) Wang, L.; Smith, D. L. *Protein Sci.* **2005**, *14* (6), 1661–1672.

(33) Gillard, J. W.; Morton, H. E.; Fortin, R.; Guindon, Y. 3-Hetero-substituted-n-benzyl-indoles and prevention of leucotriene synthesis therewith. 1992.

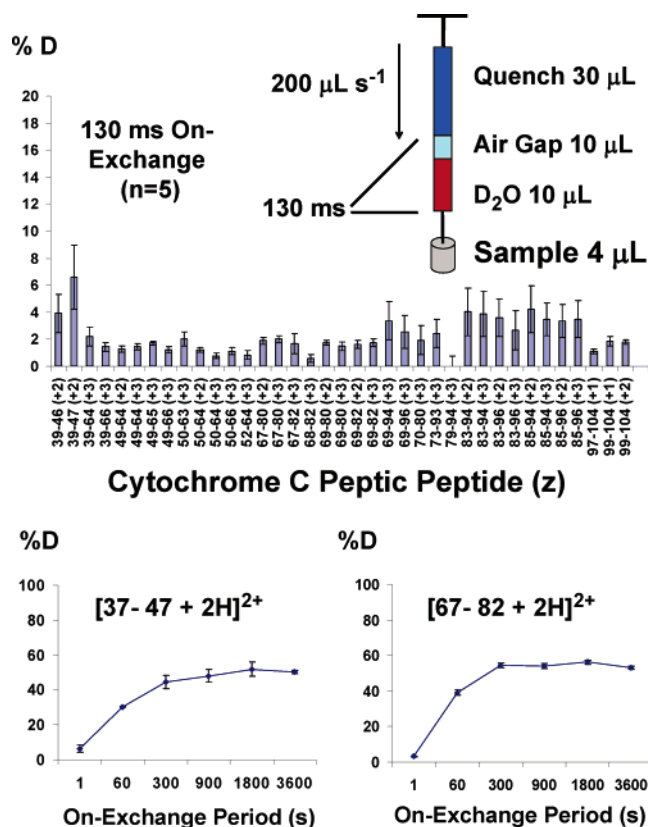


**Figure 1.** Illustrative data from the H/D exchange analysis of cytochrome *c*. (Top) Percent deuterium incorporation for 37 segments of cytochrome *c* following 130 ms on-exchange of the protein with D<sub>2</sub>O buffer. Reproducibility of the experiment was excellent, with a mean standard deviation of 0.7% over the 37 peptides ( $n = 5$  replicates). On this time scale, none of these 37 peptides had exchanged above 7%, allowing us to follow precisely the H/D exchange kinetics of rapidly exchanging peptides. (Bottom) Percentage deuterium incorporation for residues 37–47 and 67–82 after six on-exchange periods (1, 60, 300, 900, 1800, and 3600 s). Each data point shows the error in the measurement of deuterium incorporation ( $\pm$ standard deviation) over the three replicates of this experiment, again demonstrating excellent reproducibility, even for short on-exchange periods.

a delay of 50 ms prior to addition of the quench solution, yielding a total on-exchange period of  $\sim$ 130 ms. Following addition of the quench solution, the sample (50  $\mu$ L) is aspirated and transferred to the sample loop of the Trio valve.

**Long On-Exchange Periods: 15 s to 24 h.** On-exchange for periods greater than 15 s was performed as follows. PAL 2 places 4  $\mu$ L of the protein stock solution into an empty vial held at 25 °C. PAL 1 then aspirates 16  $\mu$ L of on-exchange D<sub>2</sub>O buffer and dispenses into the sample vial, after which an internal timer is started. Protein and D<sub>2</sub>O buffer solutions are mixed by repeated aspiration and dispensation. Upon completion of on-exchange period, 20  $\mu$ L of protein in on-exchange buffer is aspirated and dispensed into a vial containing 30  $\mu$ L of quench solution housed in the 1.5 °C stack. Following mixing, the sample is loaded into the injection loop of the Trio valve.

**Immobilized Enzyme Columns.** For on-line proteolytic digestion under slow-exchange conditions, columns were purchased (Porozyme Pepsin column, Applied Biosystems) or prepared in-house as detailed by Wang.<sup>34</sup>

**Linear Ion Trap Mass Spectrometry.** Linear ion trap mass spectrometry was performed with a ThermoFinnigan LTQ instrument fitted with an “ion-max” ESI source. HPLC eluent was infused into the instrument at 60  $\mu$ L min<sup>-1</sup>. For MS experiments, spectra were acquired over the range 300 <  $m/z$  < 1700. Each spectrum results from the sum of three microscans. Maximum ion fill time was 100 ms. All data were acquired in profile mode. For MS/MS experiments, a precursor ion survey scan was performed as above, and the five most abundant ions were selected for product ion analysis. Zoom scans were not acquired. The data-dependent MS/MS settings were as follows: the repeat count was set to 1, with an exclude time of 180 s. Product ion spectra resulted from the sum of three microscans and were collected in centroid mode.

**Fourier Transform Ion Cyclotron Resonance Mass Spectrometry.** For FT-ICR MS experiments, the H/D exchange system described above was transported to the National High Magnetic Field Laboratory site at Florida State University and coupled to an LTQ-FT (Thermo Electron Corp., Bremen, Germany) linear ion trap FT-ICR mass spectrometer modified for use in a 14.5-T superconducting magnet (Magnex Scientific, Oxford, U.K.).<sup>35</sup> Specifically, the octopole transfer optics and ICR cell support were lengthened to fit the larger magnet, and the two turbomolecular pumps closest to the magnet were replaced with magnetically shielded ATP 400 turbopumps (Alcatel Vacuum Products, Hingham, MA). Automated control of the number of ions delivered to the ICR cell (automatic gain control)<sup>36</sup> combined with high magnetic field results in externally calibrated mass accuracy below 1 ppm rms, even when the ion flux from the source varies by orders of magnitude (e.g., when used for LC–ESI-MS).

**Data Processing.** For peptide identification, MS/MS data files were processed with Bioworks 3.1 and submitted to SEQUEST for searching against a database containing the protein(s) of interest and pepsin. All peptide ion assignments were verified manually. Where mass accuracies are calculated, the measured  $m/z$  ratio is compared to the theoretical value calculated with IsoPro 3.1 (<http://members.aol.com/msmsoft/>). H/D exchange data were processed and visualized with software licensed from ExSAR Corp. (Monmouth, NJ).

## RESULTS AND DISCUSSION

**Automated H/D Exchange Platform.** Several aspects of the H/D exchange experiment must be evaluated to determine the capabilities of the automated system. These include but are not limited to the following: range of available on-exchange periods, reproducibility, sensitivity, sample throughput, efficiency of proteolysis, deuterium recovery, chromatographic resolution, and system robustness. Many of these are interrelated: e.g., sensitivity and chromatographic resolution improve dramatically at the cost of deuterium recovery (we define deuterium recovery as the percent deuterium measured with our apparatus for each peptide,

(34) Wang, L.; Pan, H.; Smith, D. L. *Mol. Cell. Proteomics* **2002**, *1* (2), 132–138.

(35) Hendrickson, C. L.; Blakney, G. T.; Horning, S. R.; Mackay, C. L.; Quinn, J. P.; Schaub, T. M.; Senko, M. W.; Marshall, A. G. 14.5 T Hybrid Linear Ion Trap Fourier Transform Ion Cyclotron Resonance Mass Spectrometer. In 53rd ASMS Conference on Mass Spectrometry; San Antonio, TX, 2005.

(36) Syka, J. E. P.; Marto, J. A.; Bai, D. L.; Horning, S.; Senko, M. W.; Schwartz, J. C.; Ueberheide, B.; Garcia, B.; Busby, S.; Muratore, T.; Shabanowitz, J.; Hunt, D. F. *J. Proteome Res.* **2004**, *3* (3), 621–626.

following incubation of the intact protein in 100% D<sub>2</sub>O for one month). We have evaluated all of these parameters and have standardized the system described in the Experimental Section. The overall goal was to maximize sensitivity and chromatographic resolution, while maintaining acceptable levels of deuterium recovery (>50%). However, the system is fully capable of being configured for deuterium recovery greater than 70% with concomitant reductions in sensitivity and chromatographic resolution and an increase in overall analysis time.

**H/D Exchange Kinetics.** Native protein amide H/D exchange rates can span 8 orders of magnitude.<sup>6</sup> The most rapid exchanges occur within a few milliseconds, whereas highly protected amides may require days or longer to fully exchange. Previous work demonstrated that the accuracy of H/D exchange rates calculated from MS data compares well to those obtained with NMR.<sup>30,37</sup> Here we demonstrate that our system is capable of performing precise experiments at time intervals between 130 ms and 24 h—nearly 6 orders of magnitude. The ability to make precise measurements demonstrates that we can measure perturbations in amide H/D exchange rates upon ligand binding. A recent report describes a quenched-flow setup capable of 100-ms to 30-s experiments.<sup>38</sup> However, that experimental design is limited to short on-exchange intervals, and the requirement for relatively large amount of protein limits the utility of the system. For on-exchange intervals in excess of 30 s, manual sample processing is common. However, it is extremely laborious and will affect reproducibility relative to an automated system. The system described here spans both time regimes in a single experiment.

Figure 1 contains results from H/D exchange experiments performed with horse heart cytochrome *c*. The top panel shows the measured incorporation of deuterium across 37 segments of the protein following incubation with D<sub>2</sub>O buffer for 130 ms. The average deuterium incorporation was 2.2%, with a maximum of 6.6%. The mean standard deviation ( $n = 5$  replicates) across the 37 segments was only 0.7%. Thus, we can precisely measure exchange at the low-millisecond time scale, and we can monitor H/D exchange rates for all but the most rapidly exchanging amide hydrogens. The bottom panel of Figure 1 shows deuterium exchange versus on-exchange period for two segments of cytochrome *c*. In that experiment ( $n = 3$  replicates), we performed on-exchange for 1, 60, 300, 900, 1800, and 3600 s. Again, reproducibility of the measurements was excellent throughout the duration of the experiment. The mean standard deviations for triplicate  $m/z$  measurements for 53 isotopic distributions for those on-exchange periods were  $m/z = 0.1, 0.1, 0.1, 0.2, 0.2,$  and  $0.1$ . The error bars in Figure 1 (bottom) display the standard deviation, after conversion to a percentage of the maximum theoretical deuterium incorporation, and correction for percentage deuterium in the on-exchange solution (80%) and a deuterium recovery of 50% ( $(100((\text{standard deviation}/\text{max no. exchangeable hydrogen}))/0.8)/0.5$ ).

**Chromatographic Resolution.** Following incubation of protein with D<sub>2</sub>O buffer, the sample is diluted with a cold quench solution (1.5 °C) to reduce the temperature and the pH of the solution to pH 2.5. All remaining experimental procedures are

performed as close to pH 2.5 and 1 °C as possible to minimize deuterium loss. The “slow exchange” conditions reduce the rate of exchange by  $\sim 10^6$ . However, even with careful pH and temperature control, enzymatic hydrolysis, desalting, separation, and mass spectrometric analysis must be performed within 30 min if significant levels of deuterium are to remain. To maximize chromatographic resolution (thereby reducing overlapping isotopic distributions), we perform a shallow gradient starting at 5% CH<sub>3</sub>CN, 0.3% FA, increasing to 40% CH<sub>3</sub>CN, 0.3% FA over 18 min. The limited resolving power of our linear quadrupole ion trap mass spectrometer makes the shallow gradient a necessity. FT-ICR MS fully resolves overlapping isotopic distributions (Figure 6, bottom right), enabling the use of very shallow HPLC gradients (<5 min),<sup>30</sup> and thereby reducing deuterium loss and experiment cycle time, with no loss of information.

#### Sensitivity, Deuterium Recovery, and System Robustness.

We have optimized a number of variables for increased sensitivity at the expense of deuterium recovery. For example, we use 0.3% FA in the HPLC mobile phase, not TFA. TFA is known to reduce significantly the sensitivity of ESI-MS analyses but can improve deuterium recovery. All data described in this paper were acquired with 40 pmol of protein/injection, a level comparable to a 50  $\mu\text{L min}^{-1}$  system described by Wang and Smith in 2003 (50 pmol/injection).<sup>39</sup>

For ligand screening, system robustness is more critical than sensitivity. Peptides are eluted from the HPLC column (1 mm i.d.  $\times$  1 cm long) at a relatively high flow rate of 60  $\mu\text{L min}^{-1}$ . By reducing the i.d. of the column and lowering the mobile-phase flow rate, we expect to obtain the same analyte concentration during the ESI process from a lower total amount of protein, as achieved by Wang and Smith's low flow (<1  $\mu\text{L min}^{-1}$ ) system capable of operating with 5 pmol of cytochrome *c* per injection.<sup>39</sup> However, smaller columns are more prone to failure due to clogging. Our system includes extensive back-flushing of the enzyme column, trap column, and analytical column and routinely performs multiple, triplicate, H/D exchange experiments without failure of any component. Improving the sensitivity of the system while maintaining robustness remains a primary goal and is the focus of our current efforts.

After optimizing with respect to sensitivity and robustness, we characterized the deuterium recovery of the system with replicate analysis of fully deuterated cytochrome *c*. The protein was dissolved in 100% D<sub>2</sub>O buffer and allowed to stand at room temperature for one month. Following triplicate experiments, the mean deuterium recovery for 52 segments of cytochrome *c* was 51.4% (high, 69.1%; low, 20.1%, 1.7% standard deviation). The figure in Supporting Information lists the proteolytic peptide ions detected by ESI-MS, along with percent deuterium recovery. In experiments that require higher deuterium recovery, we can modify the conditions. We were able to retain an average of 65% D<sub>2</sub>O from 21 segments of cytochrome *c* (maximum, 83%; minimum, 59%, data not shown). For this experiment we used a 6-min HPLC gradient and a 1-min digestion/desalting step (instead of the usual 3-min step) and maintained FA in the mobile phase.

**Analysis of Ligand Binding to PPAR $\gamma$ .** The glitazones, rosiglitazone and pioglitazone, target PPAR $\gamma$  and are insulin-sensitizing drugs marketed for the treatment of insulin resistance

(37) Hamuro, Y.; Coales, S. J.; Southern, M. R.; Nemeth-Cawley, J. F.; Stranz, D. D.; Griffin, P. R. *J. Biomol. Technol.* **2003**, *14* (3), 171–182.

(38) Rist, W.; Rodriguez, F.; Jorgensen, T. J. D.; Mayer, M. P. *Protein Sci.* **2005**, *14* (3), 626–632.

(39) Wang, L.; Smith, D. L. *Anal. Biochem.* **2003**, *314* (1), 46–53.

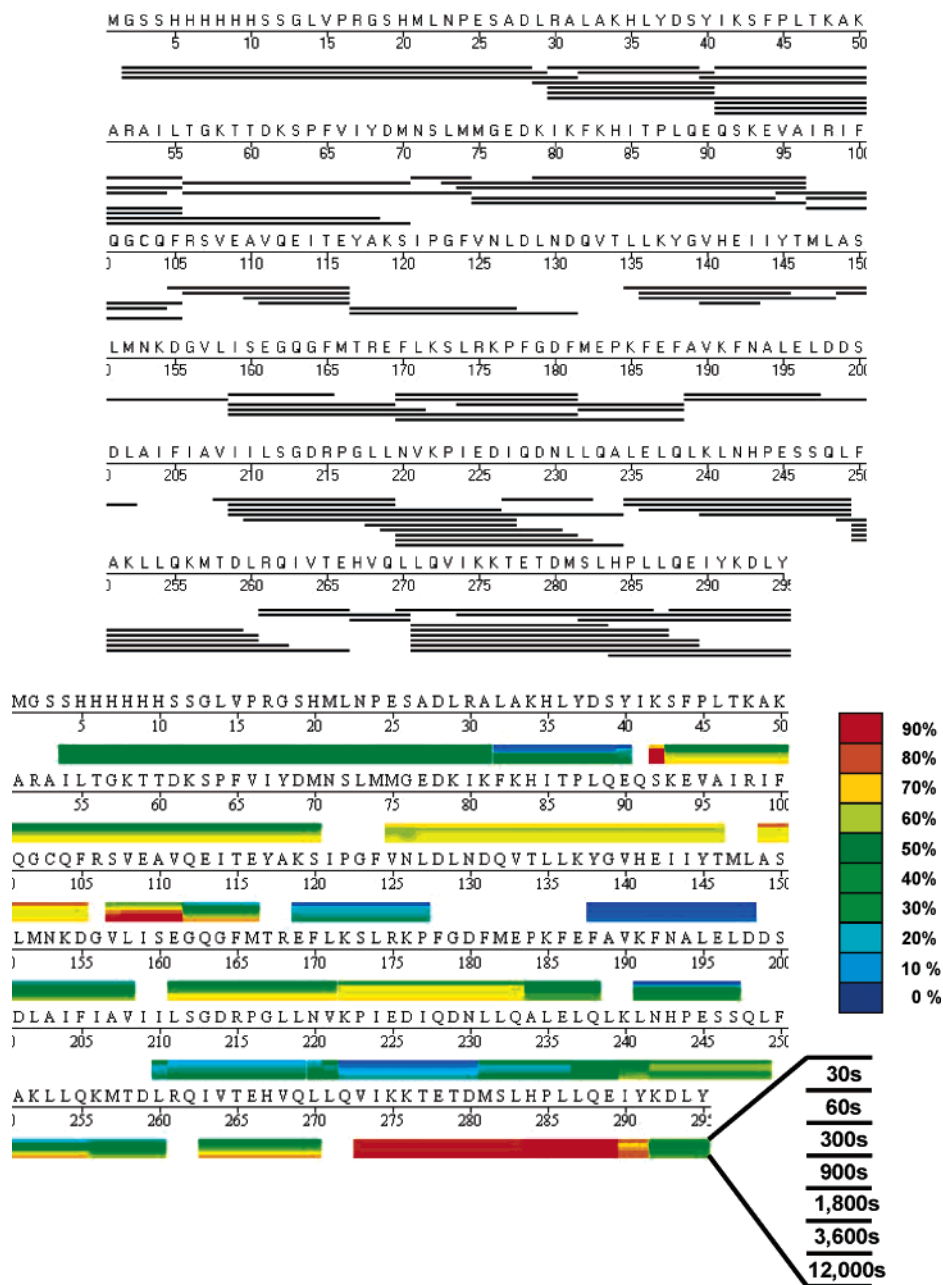


**Figure 2.** H/D exchange data for PPAR $\gamma$  LBD. (Top) Sequence coverage of PPAR $\gamma$  LBD following digestion with immobilized pepsin (~98% of LBD region covered). Amino acid numbering is for the His-tagged LBD construct, not the full length protein. Solid black lines represent proteolytic peptides followed during the H/D exchange experiment. (Bottom) On-exchange map for His-tagged apo PPAR $\gamma$  LBD. Each block represents a pepsin-generated fragment of PPAR $\gamma$  LBD detected by LC–MS and monitored during on-exchange to determine deuterium incorporation. The gradations within each block represent six on-exchange periods, with the shortest period on top. The deuteration level, as a percent of the theoretical maximum, for each peptide at each time point is color-coded (bottom right).

associated with type II diabetes. Both drugs are full agonists of the receptor. These full agonist drugs are associated with adverse effects in patients such as weight gain, edema, and plasma volume expansion.<sup>40</sup> Recently, it has been shown in animal models of type II diabetes that partial agonists of PPAR $\gamma$  are able to provide insulin-sensitizing properties similar to those of the full agonists, but without these adverse effects.<sup>40,41</sup> These and other studies have

lead to the proposed development of selective PPAR $\gamma$  modulators that maintain potent insulin sensitization activity but do not influence weight gain and plasma volume.<sup>26</sup>

We therefore performed H/D exchange to probe the nature of PPAR $\gamma$ –ligand interaction with a full agonist and a partial agonist. Since ligand activation of nuclear receptors involves conformational change in the receptor induced by ligand binding, H/D exchange is an ideal technology to probe differences

(40) Liu, K.; Black, R. M.; Acton, J. J., 3rd; Mosley, R.; Debenham, S.; Abola, R.; Yang, M.; Tschirret-Guth, R.; Colwell, L.; Liu, C.; Wu, M.; Wang, C. F.; MacNaul, K. L.; McCann, M. E.; Moller, D. E.; Berger, J. P.; Meinke, P. T.; Jones, A. B.; Wood, H. B. *Bioorg. Med. Chem. Lett.* **2005**, *15* (10), 2437–2440.

(41) Acton, J. J., 3rd; Black, R. M.; Jones, A. B.; Moller, D. E.; Colwell, L.; Doebber, T. W.; MacNaul, K. L.; Berger, J.; Wood, H. B. *Bioorg. Med. Chem. Lett.* **2005**, *15* (2), 357–362.

### (PPAR $\gamma$ LBD + GW 1929) - (PPAR $\gamma$ LBD)

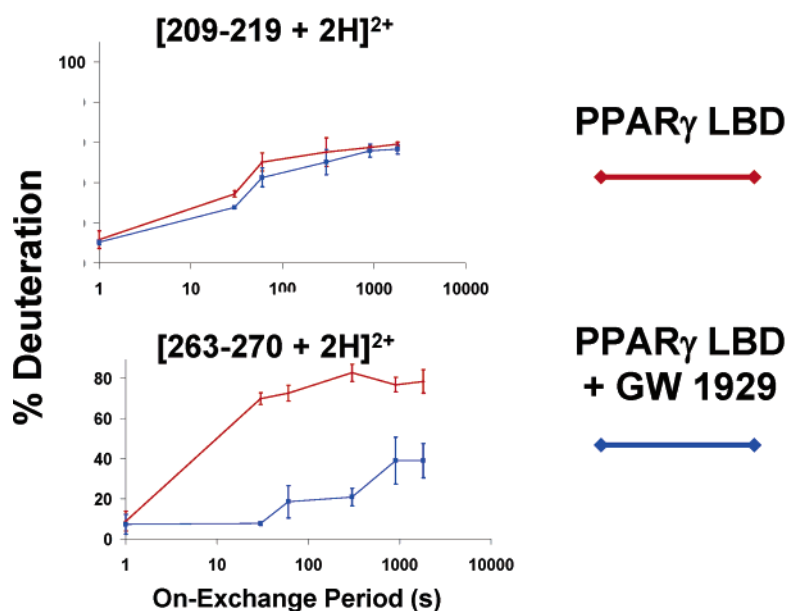
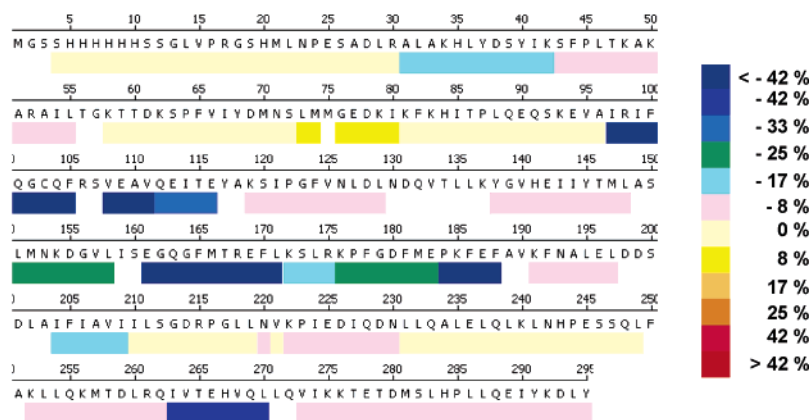


**Figure 3.** (Top) Graphical representation of the change in H/D exchange rate on binding of GW1929 to free PPAR $\gamma$  LBD receptor. (Bottom) Examples of the underlying deuterium uptake profiles. Residues 209–219 show a minimal change in H/D exchange rate upon ligand binding whereas residues 263–270 (located in helix 11) show a significant reduction in exchange rate upon binding of GW1929. This experiment was performed in triplicate, and the error bars represent the standard deviation of each measurement.

in receptor interactions between full agonists and partial agonist, a process that is difficult to measure in the context of the receptor by most structural technologies. We applied H/D exchange to classify PPAR $\gamma$  ligands as either full or partial agonists in a rapid and robust fashion by providing specific H/D exchange fingerprints for each compound. We are using this approach to develop these fingerprints as surrogates for compound behavior in an animal model of type II diabetes.

Having developed a robust automated H/D exchange system, we proceeded to investigate the changes in the PPAR $\gamma$  LBD H/D exchange rates induced by binding of GW1929 (a non-thiozolidinedione (TZD) PPAR $\gamma$  full agonist and an analogue of rosiglitazone) and nTZDpa (a non-TZD partial agonist). Figure 2 (top) shows the sequence coverage obtained for PPAR $\gamma$  LBD. Only 9 of 295 residues were not detected, providing 97% sequence coverage. Difference in H/D exchange between multiple overlapping peptides provides for increased amide resolution. Note that numbering of the amino acid sequence in Figure 2 corresponds to the PPAR $\gamma$  LBD, not full length PPAR $\gamma$ .

Figure 2 (bottom) shows the H/D exchange map obtained following triplicate analysis for on-exchange periods of 30, 60, 300, 900, 1800, 3600, and 12 000 s. Each colored block represents a specific peptide (the corresponding amino acid sequence is directly above the block), and the block is split into seven sections, one for each on-exchange period. The shortest exchange periods are on the top and increase downward. The percent exchange is calculated by dividing the measured number of deuterium atoms incorporated by the calculated number of exchangeable amide hydrogen atoms for that peptide. The calculated number of exchangeable amide hydrogen atoms equals the number of amino acid residues, minus two (one for the newly formed N-terminal amino group and one for the first amide whose exchange rate is influenced by the presence of the free amino group), minus the number of proline residues (which have no amide hydrogen to exchange). Percentage values are then corrected for the deuterium composition of the exchange solution (80%) and the average recovery of deuterium for the experiment (~55%).

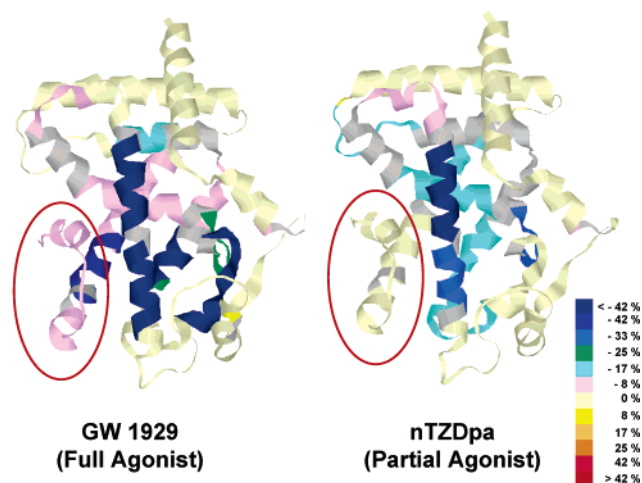


**Figure 4.** Change in H/D exchange rates for binding of a full agonist (left) and partial agonist (right) to free PPAR $\gamma$  LBD. H/D exchange perturbation data were threaded onto a PPAR $\gamma$  LBD crystal structure PRG1. Helices 11 and 12 (circled) are involved in coactivator recruitment and show significant stabilization upon binding GW1929, but no detectable stabilization upon binding of nTZDpa.

To demonstrate that we could detect changes in H/D exchange rates between free PPAR $\gamma$  LBD and ligand-bound PPAR $\gamma$  LBD, we incubated 10  $\mu$ M PPAR $\gamma$  LBD with 200  $\mu$ M GW1929 or nTZDpa for 3 h at 25  $^{\circ}$ C. Those conditions suffice to drive >99% of the PPAR $\gamma$  LBD to the ligand-bound confirmation. H/D exchange experiments were then performed in triplicate as described above, and the error bars on all figures correspond to the standard deviation of the measurement. Figure 3 (top) shows the differential H/D exchange data between free PPAR $\gamma$  LBD and PPAR $\gamma$  LBD bound to GW1929. In contrast to the data shown in Figure 2 (top), the color coding here represents the difference in area under a plot of deuterium uptake versus time (on a log scale) between the free and bound forms. Examples of the underlying data are shown in Figure 3 (bottom). The segment spanning residues 209–219 shows a minimal change in H/D exchange rate when GW1929 is bound to PPAR $\gamma$  LBD. In contrast, the segment between residues 263 and 270 shows a significant reduction in amide H/D exchange rate upon binding of GW1929. We have thus obtained an H/D exchange fingerprint for GW1929 bound to PPAR $\gamma$  LBD.

In Figure 4 we have overlaid the differential H/D exchange data from Figure 3 onto the 1PRG X-ray crystal structure for PPAR $\gamma$  LBD.<sup>42</sup> We have plotted the average percent change in exchange rates across the full range of on-exchange periods. On the left is the differential data comparing PPAR $\gamma$  LBD  $\pm$  GW1929; the right panel shows the differential data for PPAR $\gamma$  LBD  $\pm$  nTZDpa. In both cases, we see a reduction in H/D exchange rate in helix 3 (H3) (centrally located helix, dark blue). H3 is known to interact with PPAR $\gamma$  ligands, so a reduction in exchange rate in that helix can be rationalized through ligand-induced stabilization of the helix. Significant differences between the two data sets were observed. Upon binding of GW1929, helices 11 and 12 (circled) showed significant reduction in H/D exchange rate

(42) Nolte, R. T.; Wisely, G. B.; Westin, S.; Cobb, J. E.; Lambert, M. H.; Kurokawa, R.; Rosenfeld, M. G.; Willson, T. M.; Glass, C. K.; Milburn, M. V. *Nature* **1998**, *395* (6698), 137–143.

#### PPAR/RXR Heterodimer + Retinoic Acid

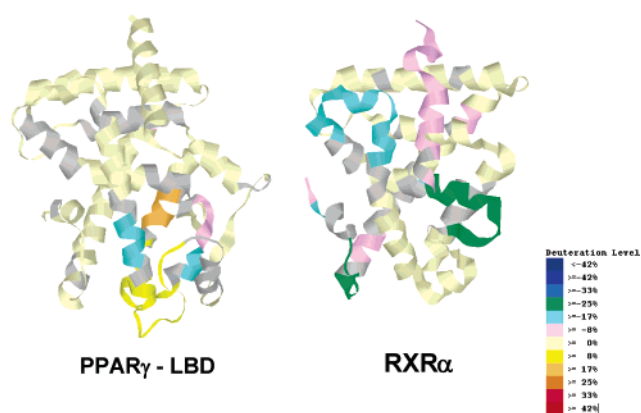


**Figure 5.** Change in H/D exchange rates upon binding 9-*cis*-RA to the PPAR $\gamma$  LBD/RXR $\alpha$  LBD heterodimer. Differences in exchange rates were observed for segments of PPAR $\gamma$  (left) and RXR $\alpha$  (right) upon binding of 9-*cis*-RA to RXR $\alpha$ . These data demonstrate that H/D exchange can detect allosteric effects of ligand binding to multiprotein complexes.

(Figure 4 (left)). However, no protection of H/D exchange was observed for H11 and H12 upon binding of the partial agonist nTZDpa (Figure 4 (right)). H11 and H12 are of particular interest because those regions of the protein are involved in coactivator recruitment to the AF-2 surface of PPAR $\gamma$ .<sup>43</sup> The rates of exchange within segments such as H11 and H12 may therefore provide the basis of a rapid and sensitive biophysical method for discriminating between full and partial PPAR $\gamma$  agonists. Currently, we are investigating the mechanism of transcriptional activation mediated by the partial agonist nTZDpa with H/D exchange analysis of the heterodimeric ligand complex, in experiments such as those described below.

**Ligand Interaction with PPAR $\gamma$ /RXR $\alpha$  LBD Heterodimer Complex.** Having demonstrated that H/D exchange analysis can detect effects of ligand binding to PPAR $\gamma$  LBD, we expanded the study to include the PPAR $\gamma$  LBD/RXR $\alpha$  LBD heterodimer complex. RXR $\alpha$  is the co-receptor for PPAR $\gamma$ , and heterodimer formation is required for transcriptional activation by PPAR $\gamma$  ligands. We applied H/D exchange to probe ligand-induced changes in this protein–protein complex to better understand the mechanism of ligand dependent activation of the heterodimer complex. Analysis of a  $\sim$ 70-kDa multiprotein complex versus a single  $\sim$ 35-kDa protein increases the analytical challenge associated with the H/D exchange experiment. The larger number of proteolytic peptides from the  $\sim$ 70-kDa complex increases the chance of overlapping peptide isotopic distributions in both chromatographic retention time and *m/z*.

H/D exchange analysis of the PPAR $\gamma$  LBD/RXR $\alpha$  LBD heterodimer complex with the linear quadrupole ion trap mass spectrometer resulted in relatively low sequence coverage and low spatial resolution of each component of the complex. However, even in the heterodimer complex, we were able to successfully measure the exchange of 51 proteolytic peptides from PPAR $\gamma$  LBD and 38 from RXR $\alpha$  LBD. To establish whether we could determine allosteric changes in H/D exchange rates across the dimer

(43) Kallenberger, B. C.; Love, J. D.; Chatterjee, V. K. K.; Schwabe, J. W. R. *Nat. Struct. Biol.* **2003**, *10* (2), 136–140.

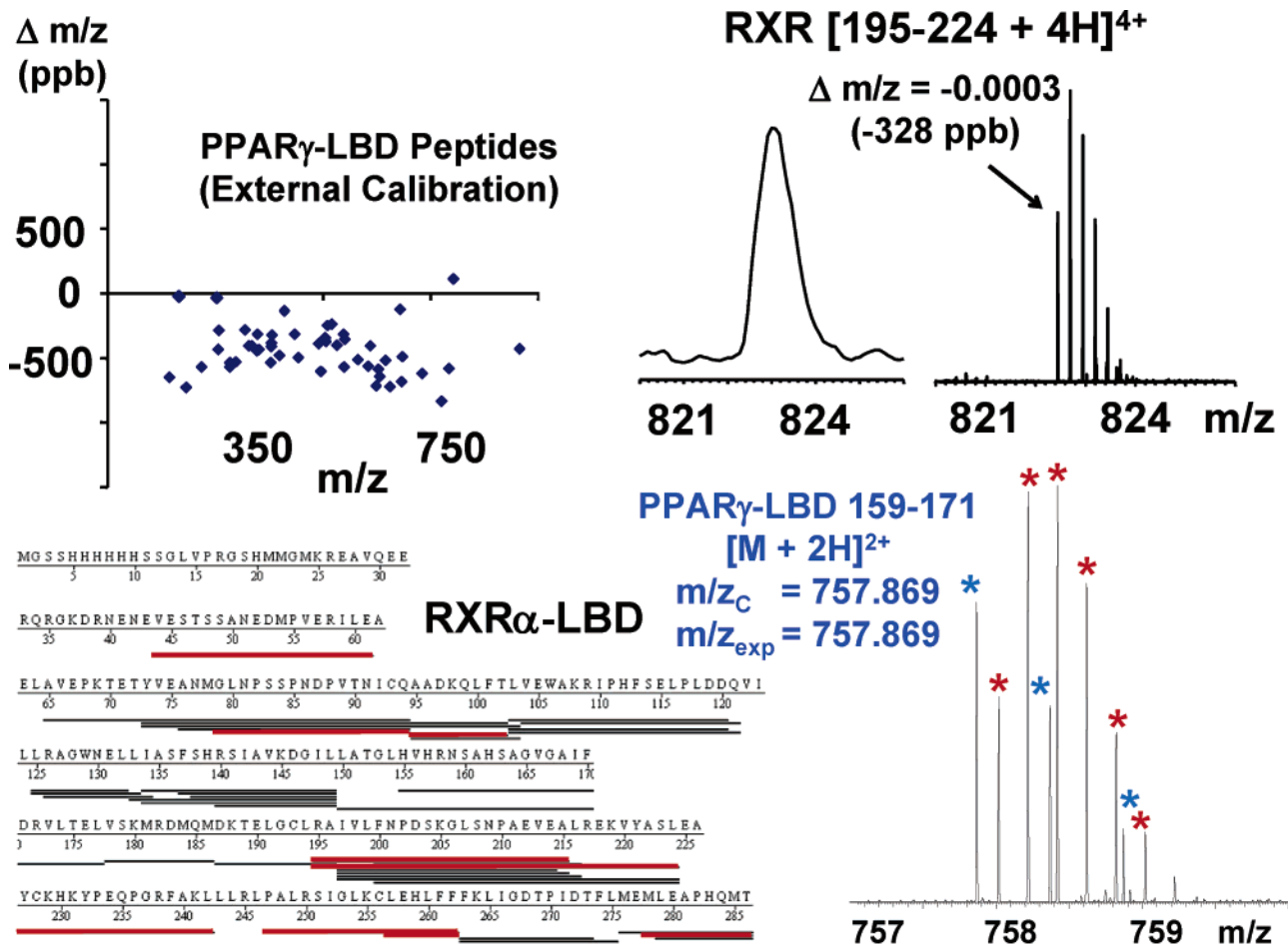


**Figure 6.** H/D exchange data for ligand binding to the PPAR $\gamma$  LBD/RXR $\alpha$  LBD heterodimer. All data were acquired with The Scripps Research Institute H/D exchange apparatus interfaced to a modified linear quadrupole ion trap 14.5-T FT-ICR mass spectrometer located at the National High Magnetic Field Laboratory. (Top left) The mean mass measurement accuracy based on external calibration for LC ESI FT-ICR MS was  $-436$  ppb for the 51 PPAR $\gamma$  LBD peptides followed in these experiments. (Top right) The high resolution of the instrument allows for the identification of previously unknown ions detected with a linear quadrupole ion trap. The additional peptides identified from the FT-ICR MS data are red in the RXR $\alpha$  LBD sequence coverage map shown in the (Bottom left) panel. Although the H/D exchange of some of the peptides identified with FT-ICR MS can be followed with our linear quadrupole ion trap, those that overlap with other isotopic distribution(s) require ESI FT-ICR MS to determine deuterium incorporation over time (bottom right).

interface, we incubated the PPAR $\gamma$  LBD/RXR $\alpha$  LBD complex with the RXR $\alpha$  agonist *9-cis*-RA. Figure 5 shows the difference in H/D exchange rates for the PPAR $\gamma$  LBD/RXR $\alpha$  LBD complex upon binding of *9-cis*-RA. The PPAR $\gamma$  LBD data are displayed on the left and the RXR $\alpha$  LBD data on the right. Both increases and decreases in the H/D exchange rates were observed for various segments of PPAR $\gamma$  LBD, even though the ligand was bound to its co-receptor RXR $\alpha$  (Figure 5 (left)). As expected, changes in H/D exchange rates were detected in segments of RXR $\alpha$  LBD upon binding of RA (Figure 5 (right)) consistent with observations by Yan and co-workers.<sup>11</sup> Thus, we have demonstrated the utility of H/D exchange to investigate allosteric effects of ligand binding to multiprotein complexes.

**14.5-T FT-ICR Mass Analysis.** Although it was possible to generate useful H/D exchange data from large multiprotein complexes with our linear quadrupole ion trap mass spectrometer, significant improvements in MS data quality are observed when the same H/D exchange apparatus was coupled to a high-field (14.5 T) FT-ICR mass spectrometer. The top left panel in Figure 6 shows errors in  $m/z$  measurement as a function of  $m/z$  for 51 PPAR $\gamma$  LBD peptide ions detected during an *externally* calibrated

LC-ESI-MS experiment. The average error was only  $-436$  ppb. Taking advantage of the resolving power of this instrument ( $m/\Delta m_{50\%} = 200\,000$  at  $m/z$  400, 1 s/MS spectrum), we were able to identify peptide ions previously unidentifiable with the linear quadrupole ion trap. An example is shown in the top right-hand panel of Figure 6; the RXR $\alpha$  [195 – 224 + 4H]<sup>4+</sup> peptide could not be identified from the linear quadrupole ion trap data; however, when analyzed under identical conditions with the FT-ICR instrument the identification was unambiguous. The charge state was established, and the error in measuring the monoisotopic peak  $m/z$  value was only  $-0.0003$  in  $m/z$  (measured  $m/z$  822.4500, calculated  $m/z$  822.4503), corresponding to an error of  $-328$  ppb. The bottom left panel details the RXR $\alpha$  proteolytic peptides (in red) that could be identified only in the FT-ICR MS experiment. Even for this small protein (35 kDa), FT-ICR MS and MS/MS provided a significant increase in the number of identified peptides. These additional peptides translate directly into increase in the spatial resolution and sequence covered by the H/D data set. In addition, the resolving power of this instrument allows identification of isotopic distributions even when they overlap (Figure 6 (bottom right)). This example shows resolution of the isotopic

distribution of PPAR $\gamma$  LBD [159 – 171 + 2H]<sup>2+</sup> that overlaps with that of an unrelated [M + 5H]<sup>5+</sup> peptide. The exchange kinetics for this peptide could not be followed without FT-ICR MS.

We have demonstrated that we can detect allosteric changes in H/D exchange rates induced through ligand binding to a multiprotein complex. The complex studied here (~70 kDa) is a heterodimer composed only of the ligand-binding domains. Our future goal is to apply H/D exchange to probe changes in exchange rates of the full length receptors and multiprotein complexes including co-activator proteins. These systems will exceed 110 kDa and will yield the most information when H/D experiments are performed with high-resolution FT-ICR mass spectrometers.<sup>14,44,45</sup>

## CONCLUSIONS

We have developed and evaluated a robust automated system for solution-phase H/D exchange capable of producing highly reproducible data for incubation periods between 130 ms and 24 h. The system was used to measure changes in H/D exchange rates for PPAR $\gamma$  LBD upon binding the full agonist GW1929 and the partial agonist nTZDpa. In contrast to GW1929, binding of nTZDpa to PPAR $\gamma$  LBD did not protect H/D exchange in segments in helix 11 or 12, both of which have been shown to be involved in coactivator recruitment in response to ligand binding. Both ligands reduced H/D exchange rates for regions of helix 3, which is known to interact with ligands such as rosiglitazone. Working with the PPAR $\gamma$  LBD/RXR $\alpha$  LBD heterodimer, we

measured allosteric changes in PPAR $\gamma$  LBD upon binding of 9-*cis*-RA to the protein complex. H/D exchange should therefore become a powerful tool for detecting ligand binding effects across components of a multiprotein complex. Studies are underway to determine the effects of partial agonist binding to the PPAR $\gamma$ /RXR $\alpha$  heterodimer. In addition, coupling H/D exchange with FT-ICR MS detection improved sequence coverage and allowed the exchange of overlapping isotopic clusters to be delineated. The use of high-resolution FT-ICR MS will become essential for H/D exchange analysis of multiprotein complexes exceeding 110 kDa.

## ACKNOWLEDGMENT

The authors thank Steve Coales (ExSAR), Yoshi Hamuro (ExSAR), and Mark Southern (ExSAR) for invaluable advice on H/D exchange experiments and automation. We also thank Tanner Schaub (NHMFL) for excellent practical help and advice regarding the 14.5-T FT-ICR. This work was supported by the NSF National High-Field FT-ICR Mass Spectrometry Facility (CHE 99-09502), Florida State University, and the National High Magnetic Field Laboratory at Tallahassee, FL. The Scripps Research Institute Florida campus is supported by the State of Florida and Florida Atlantic University.

## SUPPORTING INFORMATION AVAILABLE

Additional information as noted in text. This material is available free of charge via the Internet at <http://pubs.acs.org>.

(44) Lam, T. T.; Lanman, J. K.; Emmett, M. R.; Hendrickson, C. L.; Marshall, A. G.; Prevelige, P. E. *J. Chromatogr., A* **2002**, *982* (1), 85–95.

(45) Lanman, J.; Lam, T. T.; Emmett, M. R.; Marshall, A. G.; Sakalian, M.; Prevelige, P. E. *Nat. Struct. Mol. Biol.* **2004**, *11* (7), 676–677.

Received for review July 20, 2005. Accepted November 18, 2005.

AC051294F